Inhibition of tumor–microenvironment interaction and tumor invasion by small-molecule allosteric inhibitor of DDR2 extracellular domain

Whitney R. Grither[a,b] and Gregory D. Longmore[a,c,d,1]

[a]Integrating Communication within the Cancer Environmental Institute, Washington University, St. Louis, MO 63110; [b]Department of Biochemistry and Biophysics, Washington University, St. Louis, MO 63110; [c]Department of Medicine, Washington University, St. Louis, MO 63110; and [d]Department of Cell Biology and Physiology, Washington University, St. Louis, MO 63110

Edited by Joan Massagué, Memorial Sloan–Kettering Cancer Center, New York, NY, and approved July 10, 2018 (received for review March 22, 2018)

The action of the collagen binding receptor tyrosine kinase (RTK) discoidin domain receptor 2 (DDR2) in both tumor and tumor stromal cells has been established as critical for breast cancer metastasis. Small molecule inhibitors that target the extracellular domain of RTKs are rare, as they have classically been regarded as too small to block binding with large polypeptide ligands. Here, we report the identification and characterization of a selective, extracellularly acting small molecule inhibitor (WRG-28) of DDR2 that uniquely inhibits receptor–ligand interactions via allosteric modulation of the receptor. By targeting DDR2, WRG-28 inhibits tumor invasion and migration, as well as tumor-supporting roles of the stroma, and inhibits metastatic breast tumor cell colonization in the lungs. These findings represent an approach to inhibiting tumor–stromal interactions and support the development of allosteric inhibitors of DDR2, such as WRG-28, as a promising approach to antimetastasis treatment.

DDR2 | metastasis | allosteric inhibition

With advances in the management of local breast cancers, metastatic spread is now responsible for greater than 90% of breast cancer-related deaths. Cross-talk between tumor cells and their surrounding cellular, chemical, and physical microenvironment is now appreciated to be critical for breast tumor development, metastasis, and response to treatment (1). In breast tumors, these stromal components differ from their normal tissue counterparts in composition, architecture, and function. For example, increased collagen deposition contributes to breast density, and women with dense breasts have an increased risk for developing aggressive breast cancers (2). Moreover, excessive collagen deposition, altered collagen fiber organization, and the resulting alterations in mechanical properties of the breast tumor stroma are all correlated with more aggressive disease and poor outcome (3). Therefore, a proposed reason for the limited success of current therapies in the metastatic setting is the lack of modulating both tumor cells and the tumor microenvironment (4).

Receptor tyrosine kinases (RTKs) are well appreciated therapeutic targets for the treatment of cancer (5). The ligands that activate these receptors are typically polypeptide growth factors or cytokines, with one distinct exception—the discoidin domain receptor (DDR) family. Their ligand is fibrillar collagen, a structural protein whose expression is increased in the stroma of aggressive breast cancers (6, 7). DDRs are also unique in that their activation and inactivation kinetics are slow, and they exist as preformed dimers on the cell surface in the absence of ligands. As a result, precisely how DDR activation is regulated remains unknown. Recent human clinical data and preclinical mouse genetic models have established DDR2 as a potential therapeutic target for the metastasis of breast cancer (8), as well as many other epithelial-derived carcinomas (9–14).

In breast tumor cells, the action of DDR2 sustains their invasive and migratory capacity by sustaining the cellular level and activity of SNAIL1 in an ERK-dependent manner (9, 15). In the breast tumor stroma, the action of DDR2 in cancer-associated fibroblasts (CAFs) remodels the tumor stromal extracellular matrix (ECM) leading to a proinvasive collagen organization (8), as well as controlling CAF-secreted factors that further enhance tumor collective invasion (8). Together, these data suggest that DDR2 could be an important target for the development of inhibitors capable of modulating both the tumor cell and microenvironment, concurrently.

Most drugs targeting RTKs are of two classes. The first is receptor antibodies that block ligand binding, receptor dimerization, or receptor internalization (16, 17). The second is small molecule tyrosine kinase inhibitors (TKIs) that interact with the intracellular kinase domain (18). While TKIs inhibiting DDR2 have been identified, these compounds exhibit only a preference for DDR2 inhibition (19). Effective and lasting use of traditional TKI strategies have been hampered by the emergence of drug resistance (20), and acquired gatekeeper mutations in DDR2 treated with TKIs have already been reported (21). Therefore, development of inhibitors of DDR2 with alternative mechanisms of action could be highly advantageous.

Only recently has a small molecule allosteric regulator that targets the extracellular domain (ECD) of an RTK been described (22, 23). Allosteric or nonclassical small molecule inhibitors of RTKs offer significant therapeutic advantages (24, 25). Here, we describe the identification and characterization of

Significance

To effectively prevent cancer spread from primary tumor sites, new treatments need to target tumor cells, the cells and extracellular matrix within the tumor environment, and communicating pathways between these sites simultaneously. The collagen receptor discoidin domain receptor 2 (DDR2) has been implicated as such a target. Here, we describe the identification and characterization of a small molecule inhibitor of DDR2 that uniquely acts in an allosteric manner via the extracellular domain to selectively inhibit the action of DDR2 in tumor cells and tumor stromal cancer-associated fibroblasts. In experimental mouse models of breast cancer, WRG-28 inhibits DDR2 signaling and tumor cell invasion.

Author contributions: W.R.G. and G.D.L. designed research; W.R.G. performed research; W.R.G. and G.D.L. contributed new reagents/analytic tools; W.R.G. and G.D.L. analyzed data; and W.R.G. and G.D.L. wrote the paper.

The authors declare no conflict of interest.

This article is a PNAS Direct Submission.

[1]To whom correspondence should be addressed. Email: glongmore@wustl.edu.

This article contains supporting information online at www.pnas.org/lookup/suppl/doi:10.1073/pnas.1805020115/-/DCSupplemental.

Published online July 30, 2018.

an extracellularly acting small molecule allosteric inhibitor of DDR2 that functions to disrupt DDR2 receptor–collagen ligand interaction.

Results

Identification of a Selective, Small Molecule Inhibitor of the DDR2 ECD. To identify nonclassical inhibitors of DDR2, we adapted a DDR2 ECD binding assay (26) using plates coated with a DDR2-selective, high affinity collagen II-derived peptide (27, 28) (*SI Appendix*, Fig. S1*A*). A previous in vitro screen for DDR2 inhibitors identified the natural antibiotic, actinomycin D, as a weak inhibitor (29). By screening in the ECD binding assay, we were able to establish that actinomycin D inhibits DDR2 by acting on the extracelluar domain of the protein (Fig. 1*A*), as the kinase domain is absent in this assay. Due to its low potency and high toxicity profile (30), actinomycin D would not be considered a clinically suitable inhibitor of DDR2. Therefore, we deconstructed actinomycin D to various component chemical scaffolds to identify an active portion of the molecule, allowing for further derivatization to develop lower toxicity, higher potency inhibitors. The scaffold 7-hydroxy-phenoxazin-3-one inhibited DDR2 binding with an IC_{50} of 16 μM (Fig. 1*A* and *SI Appendix*, Fig. S1*B*). Medicinal chemistry-based optimization was performed to generate a library of lead compounds (*SI Appendix*, Figs. S1*B* and S2). One of these, WRG-28 (Fig. 1*B* and *SI Appendix*, Fig. S1*C*), showed moderate potency as an antagonist of DDR2-ligand binding (IC_{50} 230 ± 75 nM) (Fig. 1*A* and *SI Appendix*, Fig. S1*B*) and was chosen for further study.

In response to collagen I stimulation, DDR2 is activated (tyrosine phosphorylated) and leads to downstream activation of ERK to stabilize the SNAIL1 protein, thereby regulating cell migration (9). In HEK293 cells expressing DDR2, WRG-28 blunted collagen I-mediated DDR2 tyrosine phosphorylation, ERK activation, and SNAIL1 protein stabilization (IC_{50} 286 ± 124 nM) (Fig. 1 *C* and *D*). Normal mammary epithelial MCF10A cells, which do not express DDR2, were unaffected in their proliferation or survival (*SI Appendix*, Fig. S1*D*) when treated with WRG-28 (1 μM), demonstrating the absence of nonspecific toxicity from the inhibitor.

The inhibitory activity of WRG-28 was selective for DDR2. Collagen I-induced tyrosine phosphorylation of the related DDR1 RTK in HEK293 cells was unaffected by WRG-28 (*SI Appendix*, Fig. S1*E*). Further, using biolayer interferometry (BLI), we observed a dose-dependent association of WRG-28 with DDR2, but not DDR1 (*SI Appendix*, Fig. S1 *F–H*). WRG-28 did not inhibit collagen binding of α1β1 integrin ECD (*SI Appendix*, Fig. S1*I*). Finally, WRG-28 treatment did not affect phosphorylation of unrelated RTKs, as determined by RTK signaling arrays (*SI Appendix*, Fig. S3 *A* and *B*).

In summary, WRG-28 appeared to be a potent and selective inhibitor of DDR2 ECD binding to collagen in vitro, and collagen I mediated DDR2 activation in cells.

WRG-28 Inhibits DDR2–Collagen Interaction in an Allosteric Manner. Since no ECD inhibitors of DDR2 have been described, we sought to determine the mode of inhibition for WRG-28. A fluorescein-conjugated analog of the DDR2 binding collagen peptide was used to quantify the amount of substrate bound to assay plates. Fluorescein conjugation did not alter DDR2 binding to the collagen peptide (*SI Appendix*, Fig. S3*C*). In the range of substrate concentrations examined, there was linear adsorption of the DDR2 binding collagen peptide that was not reduced upon washing (*SI Appendix*, Fig. S3*D*). Using the amount of collagen peptide plated as a measure of available ligand, increasing concentration of added DDR2 ECD did not outcompete the inhibitory effects of WRG-28 (Fig. 1*E*). This suggested that WRG-28 was not acting as an orthosteric inhibitor of collagen binding.

Next, we asked whether WRG-28 displaced DDR2 from pre-bound DDR2 ECD–collagen peptide complexes. After allowing receptor–ligand complex to reach equilibrium, the complex was treated with WRG-28. In the absence of inhibitor, there was little dissociation of DDR2 over 90 min (Fig. 1*F*). However, in the presence of WRG-28, there was a dramatic acceleration of DDR2 dissociation from collagen peptide, in a dose-dependent manner (Fig. 1*F*).

Previous reports have shown that for DDR2 ECD to bind collagen, it must exist as a dimer (26) or possibly higher order multimer (31). Therefore, we asked whether WRG-28 impaired or disrupted receptor dimerization or multimerization. To do so, we made use of a DDR2 ECD protein that covalently dimerized as a result of a Fc tag added to the C terminus (DDR2-Fc) (32). In the solid phase binding assay, WRG-28's capacity to inhibit covalent DDR2-Fc dimer binding to collagen peptide was dramatically reduced (*SI Appendix*, Fig. S3*E*), suggesting that inhibition by WRG-28 may require DDR2 dimer or multimer disruption.

To determine if WRG-28 affected the organization of the DDR2 ECD in solution, we employed size exclusion chromatography. Consistent with previous reports, the majority existed as a presumed dimeric complex, while ∼20% of the DDR2 ECD eluted as a higher molecular mass oligomer, with very little monomer present (Fig. 1*G*) (26). A molecular mass calibration curve for the column was established using standard proteins of known molecular mass (*SI Appendix*, Fig. S3*G*). Monomeric DDR2 ECD runs at ∼72 kDa on SDS reducing gels. When the elution volume of the large peak was plotted using calibration curve for the column, it approximated a molecular mass consistent with a dimeric species ($K_{av} = 0.27$, M_r predicted = 154 kDa). The molecular mass of the smaller peak was estimated to be approximately double that of the dimer peak ($K_{av} = 0.44$, M_r predicted = 307 kDa), consistent with the molecular mass of an oligomeric species. When elution fractions were concentrated, run on a native gel, and compared with the DDR2 ECD protein solution added to the column, the "oligomeric" peak ran at a higher size than the dimeric peak (Fig. 1*H*). The oligomeric and dimeric peaks were collected, protein concentration normalized, and subjected to in vitro binding analysis using the solid phase assay (Fig. 1*I*). The oligomeric species bound to the collagen peptide with threefold higher affinity, illustrating the functional relevance of this higher order species. When the DDR2 ECD solution was treated with 1 μM WRG-28, the oligomer fraction was significantly reduced (Fig. 1 *G* and *J*). There appeared to be a corresponding increase in the monomeric state; however, since the monomer appeared as a shoulder of the dimer peak and was not well resolved, it could not be accurately quantified (*SI Appendix*, Fig. S3*F*).

In another approach testing whether WRG-28 could disrupt DDR2 dimers in cells, we performed chemical cross-linking of HEK293-DDR2 cells with membrane-impermeable BS^3. Consistent with previous reports, full-length DDR2 existed as dimers on the cell surface in the absence of collagen (*SI Appendix*, Fig. S3*H*) (33). When HEK293-DDR2 cells were treated with WRG-28, we did not detect significant disruption in the amount of cell surface DDR2 dimerization (*SI Appendix*, Fig. S3*H*). This could be due to the fact that in cells, full-length DDR2 dimerization is strongly influenced by the transmembrane domain (33). Regardless, WRG-28 was not capable of complete disruption of full-length DDR2 cell surface dimers.

In summary, these results indicated that WRG-28 inhibitory activity was not due to ligand-receptor binding site modulation. Rather, these results are consistent with allosteric regulation of DDR2–collagen interactions possibly due to impairment in higher order clustering of the ECD.

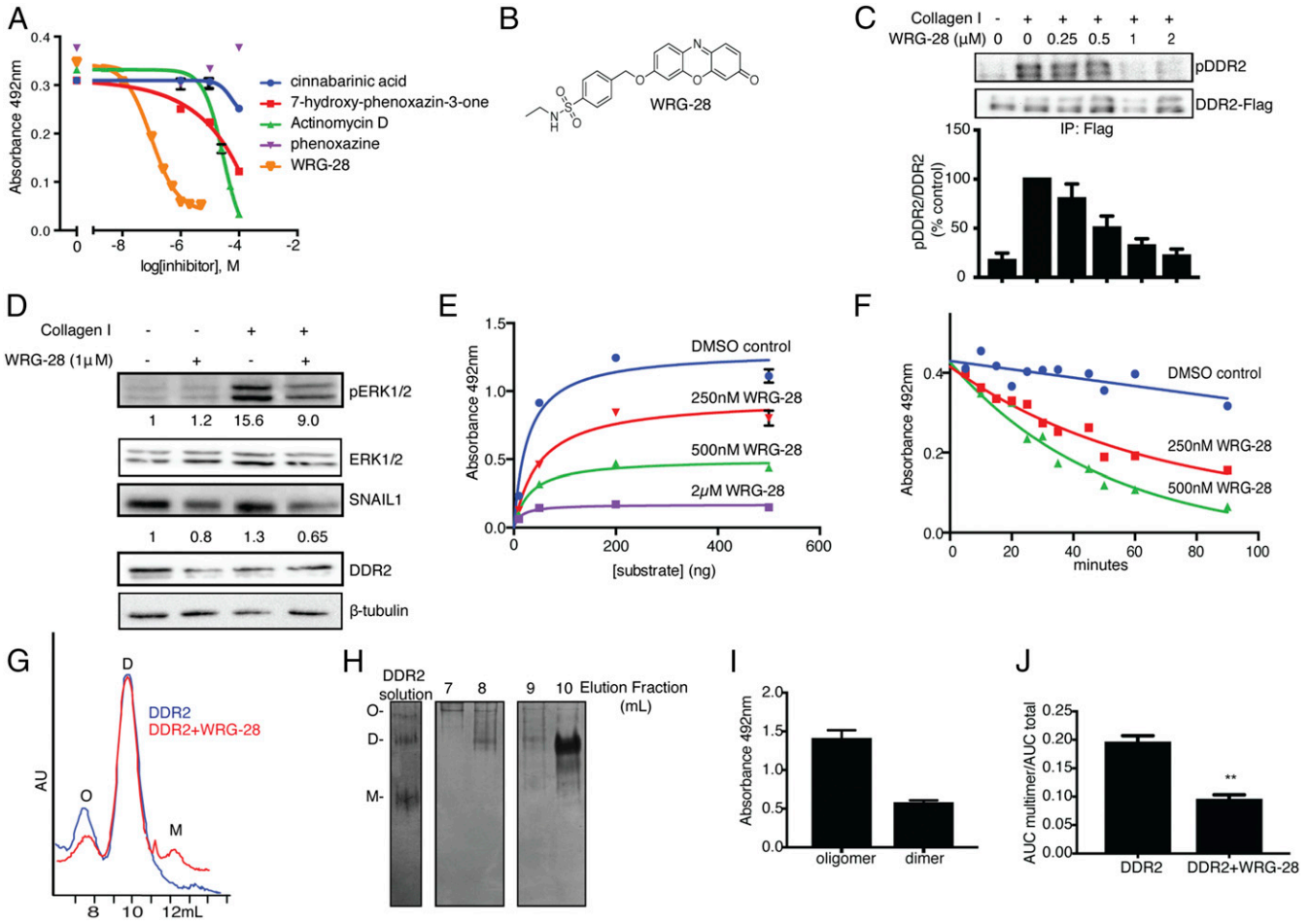

Fig. 1. Identification of DDR2 inhibitor and mode of action. (*A*) Solid-phase binding assay of 25 nM DDR2-His and 500 ng of immobilized ligand. Cinnabarinic acid (blue), 7-hydroxy-phenoxazin-3-one (red), actinomycin D (green), phenoxazine (purple), WRG-28 (orange). Graph shows mean ± SEM from a representative experiment of three independent experiments, three replicates per treatment per experiment. (*B*) Structure of *N*-ethyl-4-(((3-oxo-5a,10a-dihydro-^{3}H-phenoxazin-7-yl)oxy)methyl)benzenesulfonamide (WRG-28). (*C*) HEK293 cells transfected with DDR2-Flag were added to plates coated with 30 μg/mL collagen I for 4 h in the presence of WRG-28. DDR2 was immunoprecipitated with Flag antibody, and bound products were Western blotted with pTyr mAb 4G10 and reprobed with anti-DDR2 antibody. Densitometric quantification was performed. A representative blot was shown, quantification of five independent experiments represented as mean ± SEM. (*D*) HEK293 cells expressing DDR2-Flag were added to plates coated with 30 μg/mL collagen I for 7 h in the presence or absence of WRG-28. Western blots with the indicated antibodies were performed. Quantification of p-ERK2 and SNAIL1 are indicated on blot. (*E*) Twenty-five nanomolar DDR2-His binding in the presence of increasing concentration of collagen peptide and varying concentrations of WRG-28. DMSO control (blue), 250 nM WRG-28 (red), 500 nM WRG-28 (green), 2 μM WRG-28 (purple). Data are means ± SEM from a representative experiment of three independent experiments, three replicates per treatment per experiment. (*F*) Twenty-five nanomolar DDR2 bound to immobilized collagen peptide in solid-phase binding assay at equilibrium was exposed to a titration of compound. Graph shows dissociation of DDR2 ECD from ligand after exposure to compound at indicated concentrations for time indicated. DMSO control (blue), 250 nM WRG-28 (red), 500 nM WRG-28 (green). Data are independent time points from a representative experiment of three independent experiments. (*G*) Size exclusion chromatography. Representative elution profile of DDR2-His is shown in the presence or absence of 1 μM WRG-28 on a Superdex 200 Increase 10/300 GL column. Oligomer (O) K_{av} = 0.27, dimer (*D*) K_{av} = 0.44, monomer (M). (*H*) Native 10% PAGE fraction analysis, followed by silver staining. (*I*) Protein concentration of dimer or oligomer fractions was normalized and subjected to in vitro binding assay. Three replicates of each condition were tested, data represented as mean ± SEM. (*J*) Area under the curve was used to quantify fraction of DDR2 multimer (oligomer) compared with total DDR2. Three independent runs of each condition were quantified, data represented as mean ± SEM. $^{**}P < 0.01$.

Identification of DS-DSL Domain Interface Residues Required for DDR2–Collagen Binding and Signaling. The extracellular portion of the DDR proteins consists of three domains—an N-terminal collagen binding discoidin (DS) domain, a discoidin-like (DSL) domain, and a short membrane proximal juxtamembrane domain. The collagen binding motif in the DS domain is highly conserved between DDR1 and DDR2 (34). To gain insight into the structural determinants of DDR2 inhibition by WRG-28, SWISS-MODEL (35) was used to construct a homology model of the 3D structure of the DDR2 ECD, using the existing crystal structure of the DDR1 ECD. This structure and the resulting model contain the DS and DSL domains but lack the juxtamembrane domain (Protein Data Bank ID code 4AG4) (36). WRG-28 in silico docking analysis with AutoDock Vina (37) was performed against the homology model of DDR2. Of the top nine WRG-28 binding solutions, five low energy conformations clustered around a similar site located at the interface of the DS-DSL domains (Fig. 2*A* and *SI Appendix*, Fig. S4 *A* and *B*). Such interface binding can be a common mode of action of allosteric inhibitors (38, 39), as conformational changes along interfaces are often needed for proper receptor function (40).

In the lowest energy configuration, several key interactions were suggested (Fig. 2*B*). These included polar contacts with Arg135, Glu247, Thr98, and hydrophobic interactions with Phe96, Trp187. Residues within the interdomain region have been shown to make important interdomain contacts in the

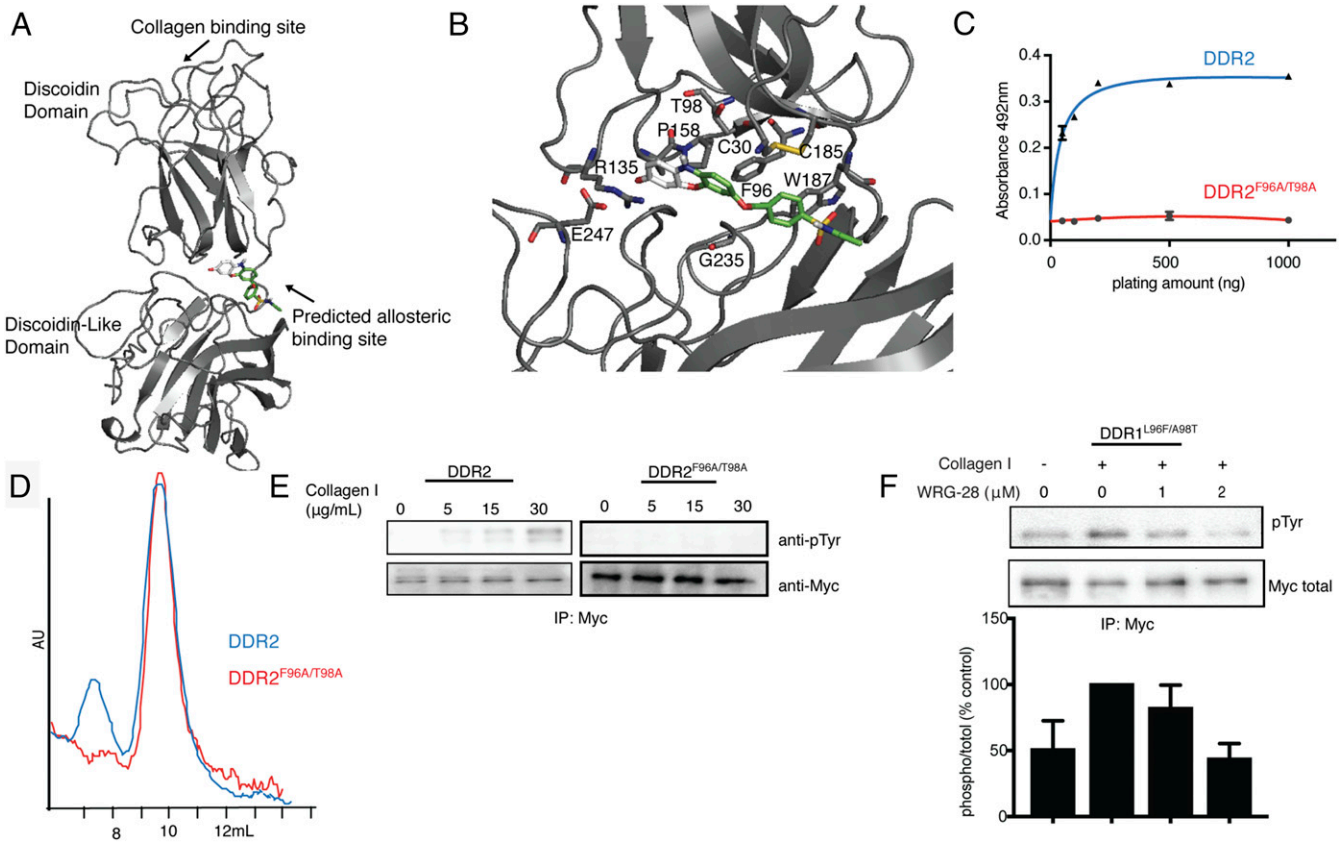

Fig. 2. Computational prediction of WRG-28 binding site and directed mutagenesis. (*A*) Overall view of the DDR2 ECD structure depicting WRG-28 in a putative binding site. (*B*) Detailed view of the predicted interactions of WRG-28. (*C*) Solid-phase binding assay of 25 nM recombinant DDR2-His or $DDR2^{F96A/T98A}$-His to the collagen peptide. (*D*) Size exclusion chromatography. Representative elution profile of DDR2-His or $DDR2^{F96A/T98A}$-His on a Superdex 200 Increase 10/300 GL column is shown. (*E*) HEK293 cells transfected with DDR2-Myc or $DDR2^{F96A/T98A}$-Myc were added to plates with indicated concentrations of collagen I for 4 h. Tagged proteins were immunoprecipitated with Myc antibody and bound products were Western blotted with pTyr 4G10 or Myc antibodies. (*F*) HEK293 cells transfected with $DDR1^{L96F/A98T}$ -Myc were added to plates coated with 30 μg/mL collagen I for 4 h in the presence of indicated concentrations of WRG-28. Tagged proteins were immunoprecipitated with Myc antibody and bound products were Western blotted with pTyr mAb 4G10 and reprobed with Myc antibodies. Representative blot is shown, quantification of three independent experiments represented as mean ± SEM.

crystallized structure of DDR1 (36). As shown, WRG-28 did not show any inhibitory activity against DDR1 (*SI Appendix*, Fig. S1*E*), despite 53% sequence identity shared between the ECDs of the two proteins. Among the interface region, two key potential interacting residues in DDR2, Phe96 and Thr98, were not conserved in DDR1 (DDR1: Leu96 and Ala98, respectively).

Single F96A or T98A point mutations in DDR2 showed no appreciable effect on DDR2 binding to collagen in vitro, DDR2 phosphorylation in cells, or inhibition by WRG-28 (*SI Appendix*, Fig. S4 *C–E*, repectively). However, $DDR2^{F96A/T98A}$ double mutant ECD protein no longer bound to collagen peptide at concentrations of ligand where binding was saturated for wild-type DDR2 ECD (Fig. 2*C*). When $DDR2^{F96A/T98A}$ ECD was analyzed by size exclusion chromatography, only the presumed dimer fraction, with virtually no higher order oligomers, was present (Fig. 2*D*). This suggested that ECD clustering may be important for collagen binding in solid phase assays. When $DDR2^{F96A/T98A}$ was expressed as a full-length receptor in HEK293 cells, it was present at the cell surface and dimerized (*SI Appendix*, Fig. S4 *F–H*). Despite this, collagen-mediated $DDR2^{F96A/T98A}$ receptor activation in cells was dramatically reduced compared with wild-type receptor (Fig. 2*E*). In controls, DDR2 mutants of alternative, lower probability WRG-28 binding sites (*SI Appendix*, Fig. S4*I*) did not affect collagen peptide binding in vitro, collagen-induced receptor phosphorylation in cells, or WRG-28 inhibitory activity (*SI Appendix*, Fig. S4 *J–M*).

As these two residues were not conserved between DDR1 and DDR2, and WRG-28 is selective for DDR2, we asked whether we could confer inhibition by WRG-28 upon DDR1 by replacing Leu96 and Ala98 residues in DDR1 with the key interacting residues of the DDR2 counterpart (Phe and Thr, respectively). When a $DDR1^{L96F/A98T}$ mutant was expressed in HEK293 cells and subjected to treatment with WRG-28, its phosphorylation in response to collagen was now diminished in the presence of WRG-28 (Fig. 2*F*), unlike wild-type DDR1 (*SI Appendix*, Fig. S1*I*).

These modeling studies, coupled with in vitro and cell-based mutagenesis experiments, indicated that the Phe96 and Thr98 residues in the DS-DSL domain interface of DDR2 are critical for receptor interaction with collagen in vitro and receptor activation in cells. While wild-type DDR1 is not inhibited by WRG-28, introducing these two residues into DDR1 was now able to confer inhibition by WRG-28 compound.

WRG-28 Inhibition of DDR2 Blunts Tumor Cell Invasion, Migration, and Tumor-Promoting Effects of CAFs. Genetic studies in vivo and cell-based studies have shown that the action of DDR2 in breast tumor cells and tumor stromal CAFs is critical for tumor invasion, migration, and metastasis without affecting proliferation (8, 9). Treatment of human BT549 and mouse 4T1 invasive breast cancer cell lines (which express endogenous DDR2) with

WRG-28 inhibited their invasion/migration in 3D collagen I and through matrigel to an extent comparable to cells RNAi-depleted of DDR2 (Fig. 3 *A* and *B* and *SI Appendix*, Fig. S5 *A*, *C*, and *G*). In both breast cancer cell lines, WRG-28 treatment also inhibited DDR2-mediated SNAIL1 protein stabilization in response to collagen stimulation (Fig. 3*C* and *SI Appendix*, Fig. S5*B*). Treatment of BT549 cells with WRG-28 did not affect their proliferation (*SI Appendix*, Fig. S5*D*).

The action of DDR2 in tumor stromal cells also plays an important role in regulation of metastasis (8). In particular, the action of DDR2 in CAFs influences their tumor-promoting function, in part, by mediating the secretion of paracrine signals that enhance collective invasiveness of tumor cells (8). To assess the ability of WRG-28 to modulate such CAF effects, primary MMTV-PyMT; $Ddr2^{+/+}$; ROSA-LSL-TdTomato or MMTV-PyMT; $Ddr2^{-/-}$; ROSA-LSL-TdTomato primary tumor organoids were isolated from breast tumors and plated in 3D collagen I with mouse CAFs, derived from MMTV-PyMT; $Ddr2^{+/+}$ or MMTV-PyMT; $Ddr2^{-/-}$ breast tumors, in the presence or absence of WRG-28 and the number of invasive organoids scored (*SI Appendix*, Fig. S6 *A*–*E*). Expression of Tomato was used to confirm that invasive foci were composed of invading tumor cells (Tomato positive) and not CAFs (Tomato negative) that had migrated to the tumors (*SI Appendix*, Fig. S6*F*). Treatment of $Ddr2^{+/+}$ tumor organoids alone with WRG-28 reduced the number of invasive tumor organoids to a level comparable to that seen with $Ddr2^{-/-}$ tumor organoids (Fig. 3*D*). Addition of $Ddr2^{+/+}$ CAFs to $Ddr2^{+/+}$ tumor organoids increased the number of invasive organoids present, as expected (8) (Fig. 3*D*). WRG-28 treatment potently reduced the number of invasive tumor organoids, to a level equivalent to that observed when $Ddr2^{-/-}$ breast tumor organoids and $Ddr2^{-/-}$ CAFs were cocultured (Fig. 3*D*). PI/annexin V staining confirmed that the reduction in invasion was not due to toxic effects of WRG-28 (*SI Appendix*, Fig. S6 *G* and *H*). These data indicated that not only did WRG-28 inhibit primary tumor organoid invasion in 3D collagen I matrices, but also the activity of DDR2 in CAFs to support invasion of primary tumor organoids.

We were surprised that WRG-28 inhibited invasion of BT549 and 4T1 breast cancer cells through Matrigel (Fig. 3*B* and *SI Appendix*, Fig. S5 *C* and *G*) since Matrigel contains mostly collagen IV, which is not a ligand for DDR2, and negligible

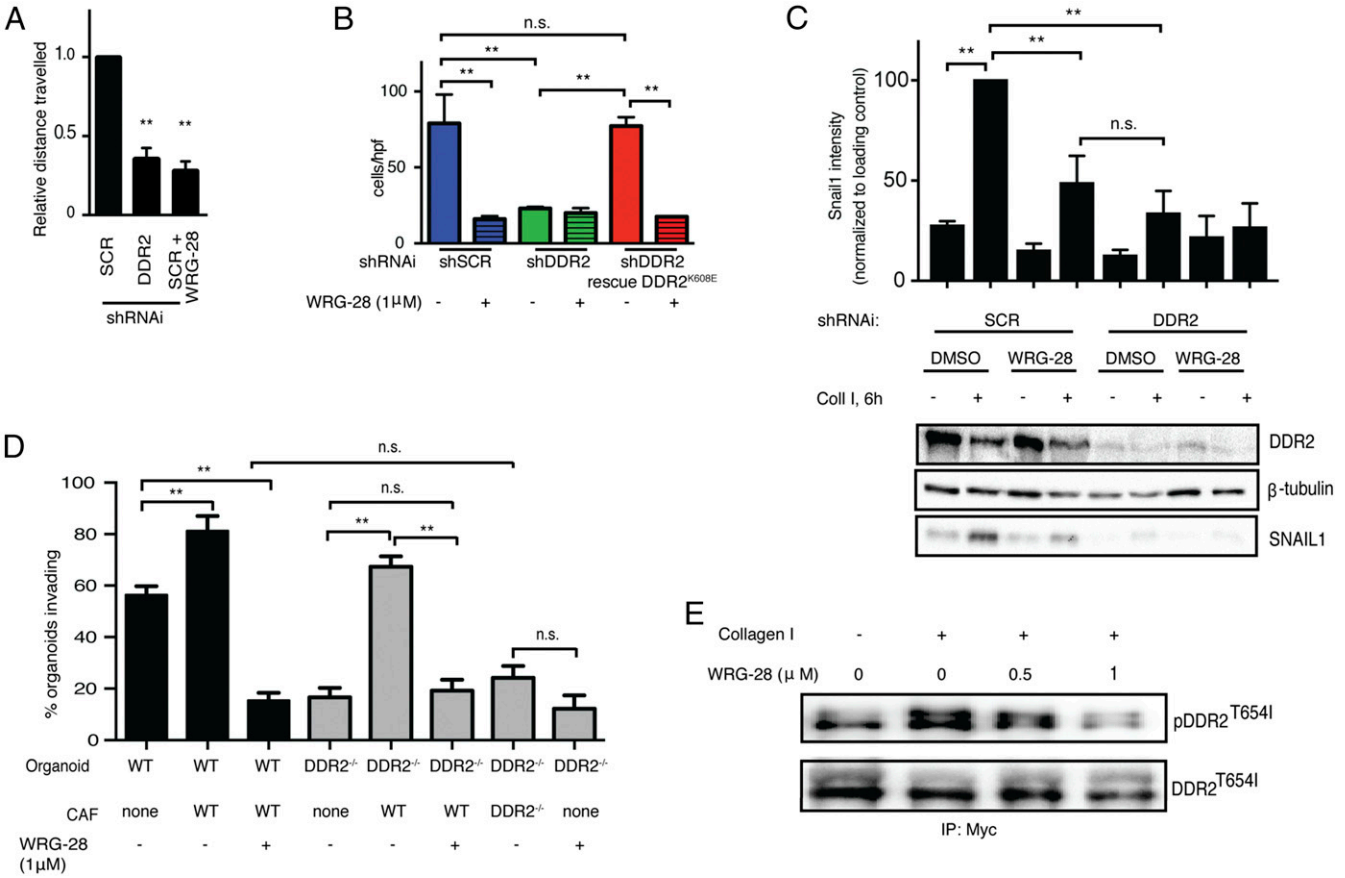

Fig. 3. WRG-28 treatment of tumor cells and CAFs. (*A*) Quantification of BT549 cell migration in 3D collagen I gels treated with 1 μM WRG-28 or control compared with cells depleted of DDR2. Distance traveled relative to control cells was determined at 48 h (**$P < 0.01$, ANOVA, $n = 4$ per condition). See also *SI Appendix*, Fig. S5*A*. (*B*) Quantification of Matrigel invasion of BT549 cell lines treated with 1 μM WRG-28 or control compared with cells shRNAi-depleted of DDR2 or depleted cells rescued with kinase dead DDR2 ($DDR2^{K608E}$) at 48 h. BT549 shSCR (blue), shDDR2 (green), or shDDR2 rescued with $DDR2^{K608E}$ (red). Striped bars indicate WRG-28 treated cells (**$P < 0.01$, ANOVA, $n = 3$ inserts per condition). Experiment was performed three independent times with similar results. See also *SI Appendix*, Fig. S5*G*. (*C*) BT549 cells added to collagen I-coated (2 mg/mL) or uncoated plates in the presence of WRG-28 (1 μM) or DMSO for 6 h. Western blots were performed with the indicated antibodies. Results were quantified by densitometric analysis of three independent experiments and represented as mean ± SEM (**$P < 0.01$, n.s, not significant, ANOVA). (*D*) Quantification of invasive tumor organoids as a percent of total organoids scored after 4 d. Thirty organoids per condition were scored. Data are mean ± SEM of a representative experiment of three independent experiments. n.s., not significant, **$P < 0.01$ one-way ANOVA. (*E*) HEK293 cells transfected with $DDR2^{T654I}$-Myc were added to plates coated with 30 μg/mL collagen I for 4 h in the presence of various concentrations of WRG-28. DDR2 was immunoprecipitated with Myc antibody and bound products were Western blotted with pTyr 4G10 or DDR2 antibodies.

amounts of fibrillar collagen (DDR2 ligand). DDR1 and DDR2 are known to be reciprocally expressed (41), and unlike DDR2, DDR1 utilizes collagen IV as a ligand. We confirmed that neither BT549 nor 4T1 cells express DDR1 at baseline. Importantly, shRNA depletion of DDR2 or treatment with WRG-28 did not induce expression of DDR1 in these cell lines (*SI Appendix*, Fig. S5*E*). Various RTKs have been shown to display kinase-independent functions within cells (42), therefore we asked if DDR2 exhibited kinase-independent functions. To do so, we rescued DDR2 expression in shRNA-depleted BT549 cells with RNAi-resistant kinase dead mutant ($DDR2^{K608E}$) (*SI Appendix*, Fig. S5*F*). $DDR2^{K608E}$ expression rescued the invasive potential of the tumor cells through Matrigel (Fig. 3*B*). Importantly, treatment with WRG-28 inhibited invasion of the $DDR2^{K608E}$-expressing cells (Fig. 3*B* and *SI Appendix*, Fig. S5*G*). In contrast, in 3D collagen I invasion assays, $DDR2^{K608E}$ rescue did not restore invasiveness (*SI Appendix*, Fig. S5*H*), indicating that the kinase-dependent action of DDR2 predominates in this assay.

Another common setback to canonical TKIs is the development of resistance mutations (20). Within the RTK family, gatekeeper mutations are a common mode of resistance, and these have been documented in DDR2 as well (21). In HEK293 cells expressing a documented DDR2 gatekeeper mutation ($DDR2^{T654I}$), WRG-28 inhibited phosphorylation of the $DDR2^{T654I}$ mutant in response to collagen I (Fig. 3*E*).

These data demonstrated that WRG-28, through its allosteric action upon the ECD, was capable of inhibiting both kinase-dependent and kinase-independent functions of DDR2. Additionally, WRG-28 maintained inhibitory action toward acquired DDR2 mutations that are resistant to TKIs.

Validation of DDR2 as a Therapeutic Target To Prevent Breast Cancer Metastasis. Ubiquitous deletion of *Ddr2* in the MMTV-PyMT mouse model of metastatic breast cancer significantly blunts lung metastases (8). While these genetic studies establish the importance of DDR2 in breast cancer metastasis, *Ddr2* was deleted from birth or shortly thereafter in such models. The potential to target DDR2 therapeutically after cancer developed and prevent metastatic disease was still unknown. To test this possibility, mice containing a conditional $Ddr2^{fl/fl}$; ROSA-$CreER^{T2}$; ROSA-LSL-TdTomato; MMTV-PyMT and control $Ddr2^{+/+}$; ROSA-$CreER^{T2}$; ROSA-LSL-TdTomato; MMTV-PyMT mice were generated. These allow for temporal deletion of $Ddr2^{fl/fl}$ during breast cancer progression upon treatment with tamoxifen.

In the MMTV-PyMT model, malignant transition occurs between 8 and 12 wk of age (43). Histologic examination of lungs at this stage showed no evidence for metastases. At 8 wk of age, mice were administered tamoxifen. Tomato fluorescence in tissues was used to document Cre activity. In mice not treated with tamoxifen, minimal tomato fluorescence was detected (*SI Appendix*, Fig. S7*A*). In mice treated with tamoxifen, the majority of cells in the breast and lung showed Tomato fluorescence (*SI Appendix*, Fig. S7*A*). In experimental mice, deletion of *Ddr2* in the tumor was confirmed by PCR (*SI Appendix*, Fig. S7*B*). In experimental and control mice, there was no difference in latency of primary tumor formation (Fig. 4*A*) or total primary tumor burden per mouse (Fig. 4*B*). However, there was a significant reduction in the number of lung metastases in mice where *Ddr2* was deleted during cancer progression (Fig. 4*C* and *SI Appendix*, Fig. S7*C*). These data support the therapeutic targeting of DDR2 in the setting of early stage breast cancer to prevent metastasis.

WRG-28 Inhibits DDR2 Signaling in Vivo and Reduces Metastatic Lung Colonization of Breast Tumor Cells. Since DDR2 signals sustain tumor cell invasion/migration through the ECM by stabilizing SNAIL1 protein level in breast tumor cells (9), we asked whether SNAIL1 level in tumors could serve as a biomarker for WRG-28 responses in vivo. 4T1 breast tumor cells that contain a SNAIL1-clic beetle green (SNAIL1.CBG) bioluminescent fusion protein that serves as a surrogate reporter of SNAIL1 protein level in tumors were implanted into the breast of syngeneic mice. After 1-cm tumors had formed, bioluminescence imaging was conducted at baseline, and WRG-28 was administered by various routes followed by bioluminescent detection of SNAIL1.CBG levels (*SI Appendix*, Fig. S7*D*). Four hours after mice were given a single i.v. administration of WRG-28 (10 mg/kg), compared with control mice, WRG-28–treated mice exhibited a 60% reduction in SNAIL1.CBG level within the tumor (Fig. 5 *A* and *B*). These data indicated that i.v. administration of WRG-28 attenuated biochemical signaling of DDR2 in breast tumors in vivo.

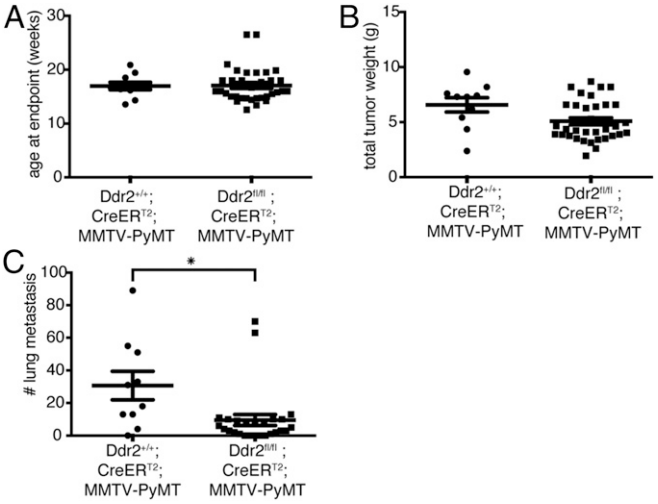

Fig. 4. Genetic validation of DDR2 as a therapeutic target. (*A*) Primary tumor growth rates of indicated mice (Ddr2 deleted at 8 wk) determined by the age at which the largest tumor reached 2 cm in diameter. $n = 10–26$ per group. Data are presented as mean ± SEM. (*B*) Total primary tumor burden of indicated mice (Ddr2 deleted at 8 wk) was determined by the sum of the weight of all tumors for each mouse when the largest tumor reached 2 cm in diameter. $n = 10–26$ per group. Data are presented as mean ± SEM. (*C*) Quantification of lung metastases in indicated mice (Ddr2 deleted at 8 wk) was calculated by the number of microscopically visible metastases from three H&E-stained sections of lung taken >200 μm apart and normalized to total lung area. $*P < 0.05$, two tailed unpaired *t* test; $n = 10–26$ mice per group. Data are presented as mean ± SEM.

To determine whether WRG-28 has the potential to inhibit metastasis in vivo, DDR2-expressing 4T1 mouse breast tumor cells expressing GFP/luciferase (4T1 GFP/luc) were injected into syngeneic BALB/cJ mice via tail vein, and lung colonization and growth were monitored by bioluminescence imaging and confirmed histologically. Genetic RNAi depletion of DDR2 in 4T1 cells significantly reduced lung metastatic colonization (Fig. 5 *C* and *D* and *SI Appendix*, Fig. S7*F*). i.v. administration of WRG-28 at 10 mg/kg daily for 7 d was chosen for dosing based on the results of SNAIL.CBG modulation by the compound (*SI Appendix*, Fig. S7*D*). WRG-28 reduced lung colonization to a level comparable to shDDR2-depleted cells (Fig. 5 *C* and *D* and *SI Appendix*, Fig. S7*F*). Histologic analysis of GFP^+ tumors in the lungs isolated at termination (7 d) confirmed the bioluminescent results (Fig. 5*E* and *SI Appendix*, Fig. S7 *E* and *G*).

A related compound, cinnabarinic acid, which is inactive as a DDR2 inhibitor in vitro (Fig. 1*A*), was also tested in this model and demonstrated no effect on lung colonization, further supporting the notion that the results of WRG-28 treatment are due to its inhibitory activity toward DDR2 (*SI Appendix*, Fig. S7*H*). While stromal DDR2 plays a critical role in the primary site in promoting the invasiveness of tumor cells (8), the role of stromal

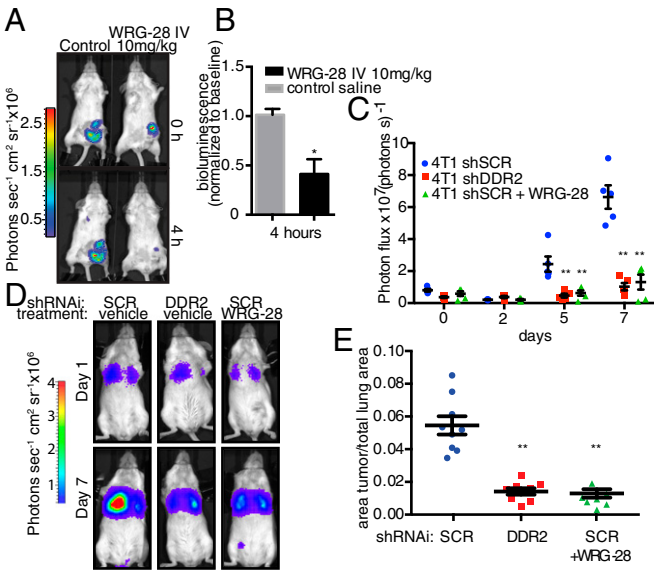

Fig. 5. WRG-28 prevention of lung colonization by metastatic breast tumor cells. (*A*) Representative bioluminescent images of 4T1-Snail-CBG tumor-bearing mice at 4 h following treatment with WRG-28 or saline control compared with pretreatment baseline. (*B*) Quantification of relative bioluminescence compared with pretreatment baseline. Mean ± SEM, $*P < 0.05$ ($n = 3$ controls, $n = 8$ treatment group). (*C*) BALB/cJ mice are injected by tail vein with 5×10^5 4T1-GFP-luc expressing cells and lungs evaluated for the presence of metastatic tumors: control (shSCR), DDR2 depleted (shDDR2), and mice injected with control cells and treated daily with WRG-28, control (blue circles); WRG-28 treated (green triangles); and shDDR2 depleted (red squares). Mean ± SEM; data derived from one experiment of five mice per condition. $**P < 0.01$ two-way ANOVA. See also *SI Appendix*, Fig. S7*F*. (*D*) Representative bioluminescent images of mice quantified in *C* following initial injection of cells and after 7 d for each experimental group. (*E*) Quantification of percentage of GFP-tumor positive area per lung at endpoint. Two sections through each of five lobes per animal quantified. Data derived from two experiments, $n = 9$ mice for each condition. Mean ± SEM, $**P < 0.001$, one-way ANOVA. See also *SI Appendix*, Fig. S7*E*.

DDR2 in the metastatic niche does not contribute to the lung colonization by breast tumor cells in this model (*SI Appendix*, Fig. S7*I*). This is consistent with the observation that treatment with WRG-28 in this assay does not confer any additional benefit beyond what is seen when shDDR2-depleted breast tumor cells are allowed to colonize. These data indicated that WRG-28 had the potential to inhibit colonization of the lung by metastatic breast tumor cells in vivo.

Discussion

We have identified a potent and selective small molecule inhibitor of DDR2. In contrast to other inhibitors, WRG-28 acts via the ECD of the receptor in an allosteric manner, potentially disrupting receptor clustering. In support of the proposed allosteric mode of action, WRG-28 is not a strong orthosteric inhibitor of ligand binding, is highly selective, dissociated preformed DDR2–collagen complexes, disrupted receptor clustering in solution, inhibited kinase-independent receptor function, and inhibited mutant DDR2 receptors resistant to traditional TKIs.

Computational modeling followed by mutagenesis analysis suggests a region at the interface of the extracellular DS and DSL domains as the putative binding site of WRG-28. In the absence of structural data, we cannot definitively confirm the predicted binding site. However, when key residues within this site are mutated ($DDR2^{F96A/T98A}$), collagen binding and DDR2 activation are abrogated, and when these residues in DDR2 (F96 and T98) were substituted into DDR1, sensitivity of DDR1 to inhibition by WRG-28 was conferred. Since WRG-28 may interfere with receptor clustering, it is possible that the binding site could be a composite site formed by two or more interacting protomers. We cannot exclude contributions from the short extracellular juxtamembrane region as it is absent from the current model.

Previous studies have suggested that receptor clustering is critical for DDR2 binding to collagen (31), and DDR1 clustering enhances activation and strengthens DDR1 binding to collagen (44, 45). If DDR2 oligomerization is required for efficient collagen binding and receptor activation, the inability of the $DDR2^{F96A/T98A}$ mutant to form higher order clusters would provide a straightforward explanation for its lack of binding and activation. We cannot exclude the possiblility that this region could function allosterically to regulate the collagen ligand binding site from a distance as have been described for integrins and other receptors (46). Alternatively, if residues within the DS-DSL domain interface region act to position two DDR2 protomers for binding and subsequent activation, these residues might contribute to conformational changes necessary for ligand binding and receptor activation.

To our knowledge, there is only one other example of a small molecule allosterically targeting the ECD of an RTK (FGFR) (22, 23). That compound inhibits signaling linked to receptor internalization in an allosteric manner without affecting orthosteric ligand binding. Although nonclassical small molecule inhibitors that disrupt protein complexes or multimerization of receptors have been reported (47, 48), to our knowledge no such inhibitors have been identified for any RTK. These types of nonclassical or allosteric inhibitors remain an elusive goal for drug development as they offer a number of favorable therapeutic attributes, such as increased selectivity and safety (24, 25). Indeed, neither the homologous family member DDR1 nor the unrelated collagen receptor α1β1 integrin is inhibited by WRG-28.

Since WRG-28 has the potential to disrupt preformed receptor complexes, this may be important for its in vivo efficacy, where the ligand (fibrillar collagen) is in great excess. WRG-28 binding to DDR2–collagen complexes appears to accelerate the intrinsically slow dissociation of the complex. Extrapolation of this in vitro data would suggest that in vivo the DDR2–collagen interaction equilibrium lies strongly in favor of receptor–ligand complex. Therefore, this mode of inhibition may be poised as advantageous over blockage of ligand binding with an orthosteric inhibitor, where an empty receptor would be needed for drug binding.

GEMMs (8) and correlative human studies (49, 50) have shown that DDR2 is important for metastasis of breast cancer through its function in both tumor cells, as well as CAFs. Therefore, DDR2 inhibition can target both the invasive tumor cell as well as stromal cells concurrently. DDR2 activation has also been implicated in other cancer types (51) as well as other disease states such as osteoarthritis (52) and cardiac (53) and pulmonary (54) fibrosis. It will be important to determine whether DDR2 inhibition with WRG-28 or derivatives would be a useful therapeutic strategy in those settings. In the context of cancer, it is important to note that genetic depletion of *Ddr2* or selective pharmacologic inhibition of the receptor does not affect primary tumor growth (8). Thus, in humans, treatment with such an antimetastasis agent would likely need to be administered as an adjuvant therapy along with standard chemotherapeutic agents that reduce tumor cell growth.

Materials and Methods

Solid-Phase Collagen-Binding Experiments. Collagens or collagen peptides were diluted in 0.01 M acetic acid coated onto Immulon 2 HB 96-well plates (Fisher Scientific) overnight at 4 °C. Wells were then blocked for 1 h at room temperature with 1 mg/mL BSA in PBS plus 0.05% Tween 20. Recombinant proteins, diluted in incubation buffer (0.5 mg/mL BSA in PBS plus 0.05%

Tween 20), were added for 3 h at room temperature. Wells were washed with incubation buffer between all incubation steps. Bound DDR2-His protein or α1β1-His were detected with anti-His–conjugated HRP monoclonal antibody (1:2,500 dilution), added for 1 h at room temperature. Bound DDR1-FC or DS2-Fc protein were detected with goat anti-human Fc coupled to horseradish peroxidase (1:2,500 dilution), added for 1 h at room temperature. Detection was achieved using *o*-phenylenediamine dihydrochloride (Sigma), added for 3–5 min. The reaction was stopped with 3 M H_2SO_4, and plates were read in a 96-well plate reader at 492 nm.

Size Exclusion Chromatography. Size exclusion chromatography was carried out at 4 °C using a BioRad Biologic Duoflow system equipped with a Superdex 200 Increase 10/300 GL column (GE). Experiments were run using PBS at a 0.5 mL/min flow rate, and elution was monitored at UV absorbance 280 nm. Twenty-five micrograms of protein were incubated in solution with 1 μM WRG-28 or DMSO for 1 h, then injected, and 1-mL fractions were collected upon elution. Fractions were concentrated using Vivaspin 500 centrifugal concentrators (10,000 molecular weight cutoff) and run on 10% gel under nonreducing conditions. To assess collagen binding of various fractions, they were immediately spin concentrated, protein concentration determined, and normalized across samples. Samples were then subjected to binding in the solid-phase plate assay.

Migration and Invasion Assays. For 3D cell migration assays, 10^5 cells were embedded in 20 μL of type I collagen gel (2.0 mg/mL) extracted from rat tail (BD Biosciences). After gelling, the plug was embedded in a cell-free collagen gel (2.0 mg/mL) within a 24-well plate. After allowing the surrounding collagen matrix to gel (1 h at 37 °C), 0.5 mL of culture medium was added on the top of the gel and cultured for another 2 d. Invasion distance from the inner collagen plug into the outer collagen gel was quantified. For invasion assays, Transwell cell invasion assays were performed using either 24-well polycarbonate membrane (Corning) with 8-μm pore size, or 24-well FluoroBlok Transwell insert (BD) with 8-μm pore size. Inserts were prepared by coating the upper surface with 1 mg/mL Matrigel (BD Biosciences) for 4–6 h at 37 °C in a 5% CO_2 incubator. BT549 or 4T1 cells (5×10^4) in DMEM containing 1% FBS were seeded into the upper chamber of the insert. The bottom chamber contained DMEM with 10% FBS. After 24 or 48 h, membranes were processed. Polycarbonate membranes were stained with HEMA3 staining kit (Fisher) and then mounted and enumerated based on number of cells per 20× high power field, five fields per insert. For FluoroBlok transwells, luminescence intensity was measured using a FluoStar Optima microplate reader (BMG Labtech) for 10 individual fields on the bottom of each insert.

Tumor Organoid and CAF Coculture. Primary tumor organoids (30–50, each 200–1,000 cells) with or without CAFs (750 cells) were cultured in 50-μL droplets of 3 mg/mL acid-solubilized rat tail collagen I (BD Biosciences), and the number of invasive organoids were enumerated daily for 4 d. Organoids were scored as invasive if they contained ≥1 protrusive projection.

Animal Studies. All procedures and care of animals were done in accordance with a protocol approved by the Washington University Institutional Animal Care and Use Committee (St. Louis, MO) and were performed in accordance with institutional and national guidelines.

Temporal Deletion of Ddr2. $Ddr2^{fl/fl}$; ROSA-LSL-TdTomato or $Ddr2^{+/+}$; ROSA-LSL-TdTomato mice were crossed to MMTV-PyMT; ROSA-$CreER^{T2}$ mice. At 8 wk, experimental and control mice were switched to 400 citrate tamoxifen-supplemented nonpelleted dry feed (Envigo) for 2 wk. Tumor-bearing mice were monitored weekly and euthanized when the largest tumor reached 2 cm in diameter. Lungs were fixed overnight in 10% formalin, cryopreserved in 30% sucrose overnight, and finally embedded in OCT and frozen in a dry ice/ethanol bath. Frozen specimens were sectioned with a cryostat (6 μm) and analyzed by fluorescence microscopy for tomato expression or stained with hematoxylin/eosin (H&E) for histological analysis. For analysis of lung metastasis, microscopically visible metastatic foci were counted from three H&E-stained sections taken 200 μm apart and reported as the total number of metastases in those three sections.

In Vivo Breast Implant Assay. Eight-week-old female BALB/cJ mice (Jackson Labs) were anesthetized. A small Y-shaped incision was made in the lower abdominal skin to expose the fourth mammary gland. 4T1-Snail.CBG cells (1×10^6) in 50 μL of DMEM were injected into the fourth mammary gland using a 29-gauge needle. The skin flaps were replaced and closed. When tumors were 1 cm in diameter, in vivo biochemical response studies were conduced by BLI at baseline, followed by i.v. lateral tail vein injection of either control saline, or indicated doses of WRG-28 in saline/DMSO, and BLI at indicated time points. The baseline BLI signal for each mouse served as its own control.

For lung metastasis formation assay, 5×10^5 cells in 100 μL of DMEM were injected into the lateral tail vein of BALB/cJ mice. Beginning on day 0, mice were treated with either control saline or 10 mg/kg WRG-28 in saline/DMSO daily for 7 d, and BLI imaging was used to follow tumor growth at time points indicated. After 7 d, mice were euthanized, and lungs were removed and fixed in 10% formalin for 24 h, cryopreserved in 30% sucrose overnight, and finally embedded in OCT and frozen in a dry ice/ethanol bath. Frozen specimens were sectioned with a cryostat (6 μm) and analyzed by fluorescence microscopy for GFP expression or stained with H&E for histological analysis.

To test the contribution of stromal DDR2 in the lung colonization assay, global deletion of DDR2 in C57BL/6 mice was achieved by backcrossing the DDR2-null allele in C57BL/6 mice for 10 generations. Heterozygote crosses generated $DDR2^{+/+}$ (wild-type) and $DDR2^{-/-}$ (null) mice for the experiment. Bo1-GFP-luc cells, a C57BL/6-derived mouse breast tumor line that is known to metastasize to lung, were injected into the lateral tail vein (5×10^5 cells in 100 μL of DMEM), and BLI imaging was used to follow tumor growth at the time points indicated.

For all BLI, mice were anesthetized with isoflurane and imaged using the IVIS 100 bioluminescent imaging system (PerkinElmer) following an i.p. injection of D-luciferin (150 mg/kg).

Extended methods can be found in the *SI Appendix*.

ACKNOWLEDGMENTS. We thank Dr. Birgit Leitinger (Imperial College London) for readily providing reagents and advice for assay development, Dr. James Janetka (Washington University in St. Louis) for providing reagents and advice with chemical synthesis, and members of the G.D.L. laboratory for helpful discussions. This work was supported by NIH Grants 5T32GM07200 (to W.R.G.), CA196205, and U54 CA210173 (to G.D.L.) and Komen Foundation Grant KG110889 (to G.D.L.).

1. Hanahan D, Coussens LM (2012) Accessories to the crime: Functions of cells recruited to the tumor microenvironment. *Cancer Cell* 21:309–322.
2. Tice JA, et al. (2013) Benign breast disease, mammographic breast density, and the risk of breast cancer. *J Natl Cancer Inst* 105:1043–1049.
3. Conklin MW, et al. (2011) Aligned collagen is a prognostic signature for survival in human breast carcinoma. *Am J Pathol* 178:1221–1232.
4. Swartz MA, et al. (2012) Tumor microenvironment complexity: Emerging roles in cancer therapy. *Cancer Res* 72:2473–2480.
5. Gschwind A, Fischer OM, Ullrich A (2004) The discovery of receptor tyrosine kinases: Targets for cancer therapy. *Nat Rev Cancer* 4:361–370.
6. Vogel W, Gish GD, Alves F, Pawson T (1997) The discoidin domain receptor tyrosine kinases are activated by collagen. *Mol Cell* 1:13–23.
7. Shrivastava A, et al. (1997) An orphan receptor tyrosine kinase family whose members serve as nonintegrin collagen receptors. *Mol Cell* 1:25–34.
8. Corsa CA, et al. (2016) The action of discoidin domain receptor 2 in basal tumor cells and stromal cancer-associated fibroblasts is critical for breast cancer metastasis. *Cell Rep* 15:2510–2523.
9. Zhang K, et al. (2013) The collagen receptor discoidin domain receptor 2 stabilizes SNAIL1 to facilitate breast cancer metastasis. *Nat Cell Biol* 15:677–687.
10. Yan Z, et al. (2014) Discoidin domain receptor 2 facilitates prostate cancer bone metastasis via regulating parathyroid hormone-related protein. *Biochim Biophys Acta* 1842:1350–1363.
11. Chua HH, et al. (2008) Upregulation of discoidin domain receptor 2 in nasopharyngeal carcinoma. *Head Neck* 30:427–436.
12. Xie B, et al. (2015) DDR2 facilitates hepatocellular carcinoma invasion and metastasis via activating ERK signaling and stabilizing SNAIL1. *J Exp Clin Cancer Res* 34:101.
13. Hammerman PS, et al. (2011) Mutations in the DDR2 kinase gene identify a novel therapeutic target in squamous cell lung cancer. *Cancer Discov* 1:78–89.
14. Xu J, et al. (2014) Overexpression of DDR2 contributes to cell invasion and migration in head and neck squamous cell carcinoma. *Cancer Biol Ther* 15:612–622.
15. Tran HD, et al. (2014) Transient SNAIL1 expression is necessary for metastatic competence in breast cancer. *Cancer Res* 74:6330–6340.
16. Arteaga CL, Engelman JA (2014) ERBB receptors: From oncogene discovery to basic science to mechanism-based cancer therapeutics. *Cancer Cell* 25:282–303.
17. Tvorogov D, et al. (2010) Effective suppression of vascular network formation by combination of antibodies blocking VEGFR ligand binding and receptor dimerization. *Cancer Cell* 18:630–640.
18. Arora A, Scholar EM (2005) Role of tyrosine kinase inhibitors in cancer therapy. *J Pharmacol Exp Ther* 315:971–979.
19. Richters A, et al. (2014) Identification of type II and III DDR2 inhibitors. *J Med Chem* 57:4252–4262.
20. Sierra JR, Cepero V, Giordano S (2010) Molecular mechanisms of acquired resistance to tyrosine kinase targeted therapy. *Mol Cancer* 9:75.

21. Beauchamp EM, et al. (2014) Acquired resistance to dasatinib in lung cancer cell lines conferred by DDR2 gatekeeper mutation and NF1 loss. *Mol Cancer Ther* 13:475–482.
22. Bono F, et al. (2013) Inhibition of tumor angiogenesis and growth by a small-molecule multi-FGF receptor blocker with allosteric properties. *Cancer Cell* 23:477–488.
23. Herbert C, et al. (2013) Molecular mechanism of SSR128129E, an extracellularly acting, small-molecule, allosteric inhibitor of FGF receptor signaling. *Cancer Cell* 23:489–501.
24. Christopoulos A (2002) Allosteric binding sites on cell-surface receptors: Novel targets for drug discovery. *Nat Rev Drug Discov* 1:198–210.
25. Wenthur CJ, Gentry PR, Mathews TP, Lindsley CW (2014) Drugs for allosteric sites on receptors. *Annu Rev Pharmacol Toxicol* 54:165–184.
26. Leitinger B (2003) Molecular analysis of collagen binding by the human discoidin domain receptors, DDR1 and DDR2. Identification of collagen binding sites in DDR2. *J Biol Chem* 278:16761–16769.
27. Carafoli F, et al. (2009) Crystallographic insight into collagen recognition by discoidin domain receptor 2. *Structure* 17:1573–1581.
28. Konitsiotis AD, et al. (2008) Characterization of high affinity binding motifs for the discoidin domain receptor DDR2 in collagen. *J Biol Chem* 283:6861–6868.
29. Siddiqui K, et al. (2009) Actinomycin D identified as an inhibitor of discoidin domain receptor 2 interaction with collagen through an insect cell based screening of a drug compound library. *Biol Pharm Bull* 32:136–141.
30. Philips FS, Schwartz HS, Sternberg SS, Tan CT (1960) The toxicity of actinomycin D. *Ann N Y Acad Sci* 89:348–360.
31. Agarwal G, Kovac L, Radziejewski C, Samuelsson SJ (2002) Binding of discoidin domain receptor 2 to collagen I: An atomic force microscopy investigation. *Biochemistry* 41:11091–11098.
32. Xu H, et al. (2011) Collagen binding specificity of the discoidin domain receptors: Binding sites on collagens II and III and molecular determinants for collagen IV recognition by DDR1. *Matrix Biol* 30:16–26.
33. Noordeen NA, Carafoli F, Hohenester E, Horton MA, Leitinger B (2006) A transmembrane leucine zipper is required for activation of the dimeric receptor tyrosine kinase DDR1. *J Biol Chem* 281:22744–22751.
34. Fu HL, et al. (2013) Discoidin domain receptors: Unique receptor tyrosine kinases in collagen-mediated signaling. *J Biol Chem* 288:7430–7437.
35. Guex N, Peitsch MC, Schwede T (2009) Automated comparative protein structure modeling with SWISS-MODEL and Swiss-PdbViewer: A historical perspective. *Electrophoresis* 30(Suppl 1):S162–S173.
36. Carafoli F, et al. (2012) Structure of the discoidin domain receptor 1 extracellular region bound to an inhibitory Fab fragment reveals features important for signaling. *Structure* 20:688–697.
37. Trott O, Olson AJ (2010) AutoDock Vina: Improving the speed and accuracy of docking with a new scoring function, efficient optimization, and multithreading. *J Comput Chem* 31:455–461.
38. Chen YN, et al. (2016) Allosteric inhibition of SHP2 phosphatase inhibits cancers driven by receptor tyrosine kinases. *Nature* 535:148–152.
39. Calleja V, Laguerre M, Parker PJ, Larijani B (2009) Role of a novel PH-kinase domain interface in PKB/Akt regulation: Structural mechanism for allosteric inhibition. *PLoS Biol* 7:e17.
40. Amemiya T, Koike R, Fuchigami S, Ikeguchi M, Kidera A (2011) Classification and annotation of the relationship between protein structural change and ligand binding. *J Mol Biol* 408:568–584.
41. Borza CM, Pozzi A (2014) Discoidin domain receptors in disease. *Matrix Biol* 34: 185–192.
42. Rauch J, Volinsky N, Romano D, Kolch W (2011) The secret life of kinases: Functions beyond catalysis. *Cell Commun Signal* 9:23.
43. Lin EY, et al. (2003) Progression to malignancy in the polyoma middle T oncoprotein mouse breast cancer model provides a reliable model for human diseases. *Am J Pathol* 163:2113–2126.
44. Coelho NM, et al. (2017) Discoidin domain receptor 1 mediates myosin-dependent collagen contraction. *Cell Rep* 18:1774–1790.
45. Yeung D, Chmielewski D, Mihai C, Agarwal G (2013) Oligomerization of DDR1 ECD affects receptor-ligand binding. *J Struct Biol* 183:495–500.
46. Changeux JP, Christopoulos A (2016) Allosteric modulation as a unifying mechanism for receptor function and regulation. *Cell* 166:1084–1102.
47. He MM, et al. (2005) Small-molecule inhibition of TNF-alpha. *Science* 310:1022–1025.
48. Berg T (2003) Modulation of protein-protein interactions with small organic molecules. *Angew Chem Int Ed Engl* 42:2462–2481.
49. Zhang K, et al. (2012) Lats2 kinase potentiates Snail1 activity by promoting nuclear retention upon phosphorylation. *EMBO J* 31:29–43.
50. Toy KA, et al. (2015) Tyrosine kinase discoidin domain receptors DDR1 and DDR2 are coordinately deregulated in triple-negative breast cancer. *Breast Cancer Res Treat* 150:9–18.
51. Valiathan RR, Marco M, Leitinger B, Kleer CG, Fridman R (2012) Discoidin domain receptor tyrosine kinases: New players in cancer progression. *Cancer Metastasis Rev* 31:295–321.
52. Manning LB, Li Y, Chickmagalur NS, Li X, Xu L (2016) Discoidin domain receptor 2 as a potential therapeutic target for development of disease-modifying osteoarthritis drugs. *Am J Pathol* 186:3000–3010.
53. George M, Vijayakumar A, Dhanesh SB, James J, Shivakumar K (2016) Molecular basis and functional significance of angiotensin II-induced increase in discoidin domain receptor 2 gene expression in cardiac fibroblasts. *J Mol Cell Cardiol* 90:59–69.
54. Zhao H, et al. (2016) Targeting of discoidin domain receptor 2 (DDR2) prevents myofibroblast activation and neovessel formation during pulmonary fibrosis. *Mol Ther* 24:1734–1744.